

INCB050465 (Parsaclisib), a Novel Next-Generation Inhibitor of Phosphoinositide 3-Kinase Delta (PI3K#)

Eddy W Yue, Yun-Long Li, Brent Douty, Chunhong He, Song Mei, Brian Wayland, Thomas Maduskuie, Nikoo Falahatpisheh, Richard B. Sparks, Padmaja Polam, Wenyu Zhu, Joseph Glenn, Hao Feng, Ke Zhang, Yanlong Li, Xin He, Kamna Katiya, Maryanne Covington, Patricia Feldman, Niu Shin, Kathy He Wang, Sharon Diamond, Yu Li, Holly K Koblisch, Leslie Hall, Peggy Scherle, Swamy Yeleswaram, Chu-Biao Xue, Brian Metcalf, Andrew P Combs, and Wenqing Yao

ACS Med. Chem. Lett., **Just Accepted Manuscript** • DOI: 10.1021/acsmchemlett.9b00334 • Publication Date (Web): 17 Oct 2019

Downloaded from pubs.acs.org on October 20, 2019

Just Accepted

“Just Accepted” manuscripts have been peer-reviewed and accepted for publication. They are posted online prior to technical editing, formatting for publication and author proofing. The American Chemical Society provides “Just Accepted” as a service to the research community to expedite the dissemination of scientific material as soon as possible after acceptance. “Just Accepted” manuscripts appear in full in PDF format accompanied by an HTML abstract. “Just Accepted” manuscripts have been fully peer reviewed, but should not be considered the official version of record. They are citable by the Digital Object Identifier (DOI®). “Just Accepted” is an optional service offered to authors. Therefore, the “Just Accepted” Web site may not include all articles that will be published in the journal. After a manuscript is technically edited and formatted, it will be removed from the “Just Accepted” Web site and published as an ASAP article. Note that technical editing may introduce minor changes to the manuscript text and/or graphics which could affect content, and all legal disclaimers and ethical guidelines that apply to the journal pertain. ACS cannot be held responsible for errors or consequences arising from the use of information contained in these “Just Accepted” manuscripts.

INCB050465 (Parsaclisib), a Novel Next-Generation Inhibitor of Phosphoinositide 3-Kinase Delta (PI3K δ)

Eddy W. Yue,^{*} Yun-Long Li,^a Brent Douty, Chunhong He, Song Mei, Brian Wayland,^b Thomas Maduskuie, Nikoo Falahatpisheh, Richard B. Sparks, Padmaja Polam, Wenyu Zhu, Joseph Glenn, Hao Feng, Ke Zhang, Yanlong Li, Xin He, Kamna Katiyar, Maryanne Covington, Patricia Feldman, Niu Shin, Kathy He Wang, Sharon Diamond, Yu Li, Holly K. Koblisch, Leslie Hall, Peggy Scherle, Swamy Yeleswaram, Chu-Biao Xue, Brian Metcalf, Andrew P. Combs, and Wenqing Yao

Incyte Research Institute, Incyte Corporation, 1801 Augustine Cut-Off, Wilmington, Delaware 19803, United States

ABSTRACT: A medicinal chemistry effort focused on identifying a structurally diverse candidate for phosphoinositide 3-kinase delta (PI3K δ) led to the discovery of clinical candidate INCB050465 (**20**, parsaclisib). The unique structure of **20** contains a pyrazolopyrimidine hinge-binder in place of a purine motif that is present in other PI3K δ inhibitors, such as idelalisib (**1**), duvelisib (**2**), and INCB040093 (**3**, dezapelisib). Parsaclisib (**20**) is a potent and highly selective inhibitor of PI3K δ with drug-like ADME properties that exhibited an excellent in vivo profile as demonstrated through pharmacokinetic studies in rats, dogs, and monkeys and through pharmacodynamic and efficacy studies in a mouse Pfeiffer xenograft model.

KEYWORDS: *Parsaclisib, INCB050465, PI3K δ , phosphoinositide 3-kinase delta, dezapelisib, INCB040093*

^aDeceased 4/20/2016

^bDeceased 5/27/2018

Phosphoinositide 3-kinase delta (PI3K δ) is a lipid kinase that phosphorylates the D-3 position of the inositol ring of phosphoinositides.¹ By acting as a downstream mediator of signaling from receptor tyrosine kinases, including the B-cell receptor, Toll-like receptors, and cytokine receptors,² PI3K δ plays a primary role in PI3K-AKT-mTOR pathway activation. When dysregulated, PI3K δ can lead to the development of hematologic malignancies including acute myeloid leukemia³ and chronic lymphocytic leukemia.⁴ PI3K δ is also central in the regulation of immune cell function (e.g., B cells, T cells, neutrophils, and mast cells),^{2,5} and PI3K δ activation therefore may promote B-cell malignancies via both direct tumor and immunomodulatory mechanisms. Importantly, by the same virtue, PI3K δ is also garnering interest as a therapeutic target in inflammatory respiratory diseases (e.g., chronic obstructive pulmonary disorder, asthma), autoimmune diseases (e.g., systemic lupus erythematosus, rheumatoid arthritis, type 1 diabetes), and activated PI3K δ syndrome.^{2,6,7} As such, there are currently intense efforts towards identifying inhibitors of PI3K δ to treat hematologic malignancies as well as other cancers and immunologic diseases.

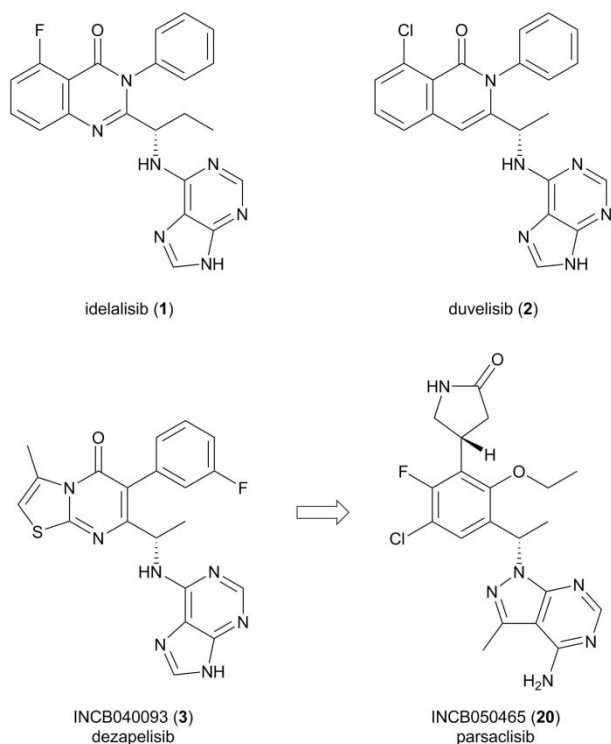


Figure 1. Structures of idelalisib (**1**), duvelisib (**2**), INCB040093 (**3**, dezapelisib), and INCB050465 (**20**, pargaclisib).

The first PI3Kδ-selective inhibitor, idelalisib (**1**), was approved for the treatment of hematologic malignancies (Figure 1).^{8,9} More recently, duvelisib (**2**), an inhibitor of both PI3Kδ and PI3Kγ, was also approved for the same indications.¹⁰ The efforts at Incyte to find a selective inhibitor of PI3Kδ led initially to INCB040093¹¹ (**3**, dezapelisib). Dezapelisib (**3**) was advanced into clinical trials for the treatment of patients with previously treated B-cell malignancies.¹² Even though these compounds demonstrate proof-of-concept that inhibition of PI3Ks are effective in treating cancer, the clinical trials of **1**, **2**, and **3** all revealed similar liver toxicity that have limited their full potential and there remains a need to develop alternative inhibitors with better safety profiles.¹³⁻¹⁵

Dezapelisib (**3**) is a potent inhibitor of PI3Kδ ($IC_{50} = 3.4$ nM) with very good selectivity over the other isoforms of PI3K and over 200 other kinases,¹¹ and it displayed cellular activity in SU-DHL-6 viability ($IC_{50} = 18$ nM) and Pfeiffer proliferation ($IC_{50} = 14$ nM) assays (Table 1). To estimate the clinical plasma concentration (total drug) needed to achieve half maximal inhibitory concentration (IC_{50}), the IC_{50} value from the Pfeiffer cell assay was corrected for the fraction unbound in media to approximate IC_{50} , and then corrected for the fraction unbound in human plasma. The calculated protein binding adjusted (PB_{adj}) IC_{50} in the Pfeiffer assay further supported **3** was indeed a potent inhibitor of PI3Kδ.

The pharmacokinetic (PK) studies of **3** in cynomolgus monkey (cyno) demonstrated that **3** exhibited good oral exposure (AUC of 4.9 $\mu M \cdot h$ dosed at 10 mg/kg), but also had a short half-life (1.3 h). Improvements in potency, PK, and toxicity were the goals of a second-generation inhibitor of PI3Kδ. As a result of the encouraging properties outlined above, **3** provided a good starting point to explore structurally diverse scaffolds. These studies culminated with the design of

INCB050465 (**20**, pargaclisib), a highly potent and selective PI3Kδ inhibitor that is currently in clinical trial studies for diffuse large B-cell lymphoma (DLBCL),¹⁶ follicular lymphoma,¹⁷ marginal zone lymphoma,¹⁸ and mantle cell lymphoma.¹⁹ Described herein are the obstacles that were encountered and the solutions that were found which eventually led to **20**.

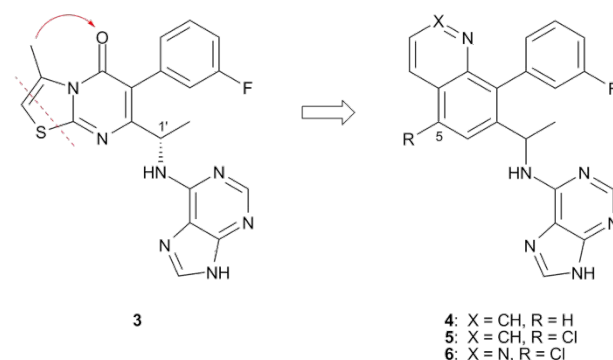


Figure 2. Design of quinoline and cinnoline inhibitors **4-6**.

One of the first ideas examined was to create a new core by breaking the thiazole ring of **3** and forming a new 6,6-bicyclic heterocycle (Figure 2) while maintaining the purine hinge-binder that was needed for PI3Kδ potency. The nitrogen in the quinoline ring (**4**) was designed to replace binding pocket interactions from the carbonyl oxygen of **3**. The synthesis of this purine series provided analogs that were either racemic or scalemic. For all single isomer compounds, the stereogenic center was assigned to be the same stereochemistry as C-1' of **3** (the opposite enantiomer was known to be inactive). The stereochemistry of **3** was assigned *S* based on the X-ray crystal structure data of an intermediate (unpublished data). Quinoline **4** was significantly less active compared with **3** (Table 1). It was hypothesized that potency could be restored by introducing small lipophilic groups at the 5-position of the quinoline ring to mimic the removed thiazole ring. In particular, chloro-substitution (**5**) dramatically improved the potency of **4** ($IC_{50} = 8.4$ nM vs 430 nM). Compound **5** was similarly potent to **3** but the low free fraction in human plasma of **5** translated into a PB_{adj} IC_{50} in the Pfeiffer assay that was 15-fold less potent than **3**. Introducing more polarity to the quinoline ring with the addition of one nitrogen at the 2-position of quinoline **5** gave cinnoline **6**. Compound **6** displayed better human plasma free fraction, higher Caco2 permeability (Supporting Information, Table S15), and similar potency compared with **5**. While **6** still exhibited a higher PB_{adj} IC_{50} in the Pfeiffer assay compared with **3**, this was offset with improved rat PK that revealed an increase in oral exposure (AUC of 13 $\mu M \cdot h$ (**6**) vs AUC of 4.4 $\mu M \cdot h$ (**3**) for same dose of 5 mg/kg). Even though the potency of **6** was weaker compared with **3**, the improvements in PK with **6** warranted further advancement. Unfortunately, **6** exhibited toxicity when dosed in dogs and its progression was halted.

Unsuccessful attempts to find alternative bicyclic cores with better potency or properties as the cinnoline led to the design of inhibitors that featured a monocyclic core ring instead of a bicyclic ring. Opening the pyridazine ring of cinnoline **6** (Figure 3) and installing a cyano group at the 3-position of the resultant phenyl ring provided **7**. While **7** was less potent than **6** toward PI3Kδ in binding and cellular assays, structure-activity relationship (SAR) studies revealed that replacement of

the cyano group in **7** with a heteroaryl group could impact potency significantly. The methylpyrazole group of **8** afforded improved potency in binding and cellular assays compared with **7**. Although **8** was very potent, two aromatic groups adjacent to each other

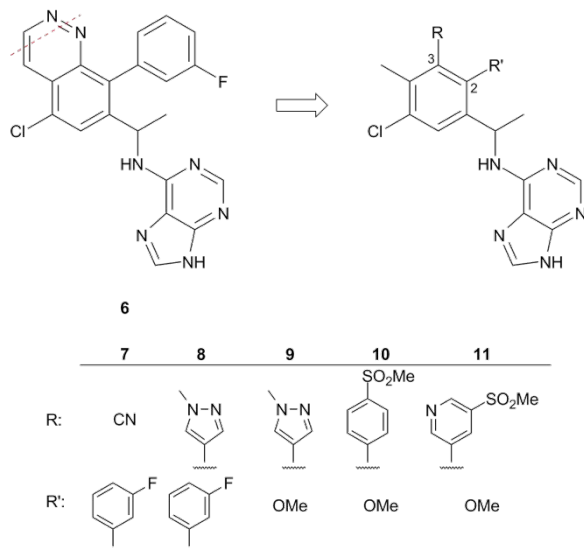


Figure 3. Monocyclic purine inhibitors **7-11**.

on the phenyl ring was believed to be less than ideal for achieving the physical properties needed for a drug candidate. SAR studies at the 2-position of the phenyl ring revealed that the solvent exposed 3-fluorophenyl group could be significantly simplified to the methoxy ether **9** without loss of potency in the enzyme binding assay.

Truncating the phenyl group to methoxy at the 2-position enabled an expanded examination of SAR at the 3-position. Substitution of the pyrazole ring for the sulfonyl phenyl analog **10** afforded similar potency with acceptable Caco2 permeability and human intrinsic clearance (hIntCl) values (Supporting Information, Table S15). Unfortunately, **10** had low free fraction in human plasma which translated into a very high $PB_{adj} IC_{50}$ in the Pfeiffer assay ($IC_{50} = 3100$ nM). The more polar pyridyl analog **11** provided a 9-fold improvement in human plasma free fraction compared with **10**. The oral exposure of **11** in rat PK was not as good as **6** (AUC of $13 \mu M \cdot h$ (**6**) vs AUC of $3.0 \mu M \cdot h$ (**11**) for same dose of 5 mg/kg) which could have been caused by the low Caco2 permeability (0.5×10^{-6} cm/s) of **11**. While many analogs were prepared in this series, finding the right balance of properties remained a challenge. Using the monocyclic phenyl core, alternative hinge-binders were considered as a potential solution.

The purine hinge-binder was replaced with 4,6-diaminopyrimidine-5-carbonitrile (Figure 4), which proved to be an effective substitute. Compound **12** offered a slight enhancement in potency compared with **11** but also a large improvement in Caco2 permeability (7.9 vs 0.5×10^{-6} cm/s). Taken together these properties delivered excellent oral exposure in rat PK (AUC of $10 \mu M \cdot h$ dosed at 4 mg/kg) for **12**. Unfortunately, **12** had elevated levels of inhibition in the HEK293 and hERG counter screens (Supporting Information, Table S14). The strategy to reduce HEK293 and hERG inhibition with polar amide groups resulted in the examination of a variety of pyridyl

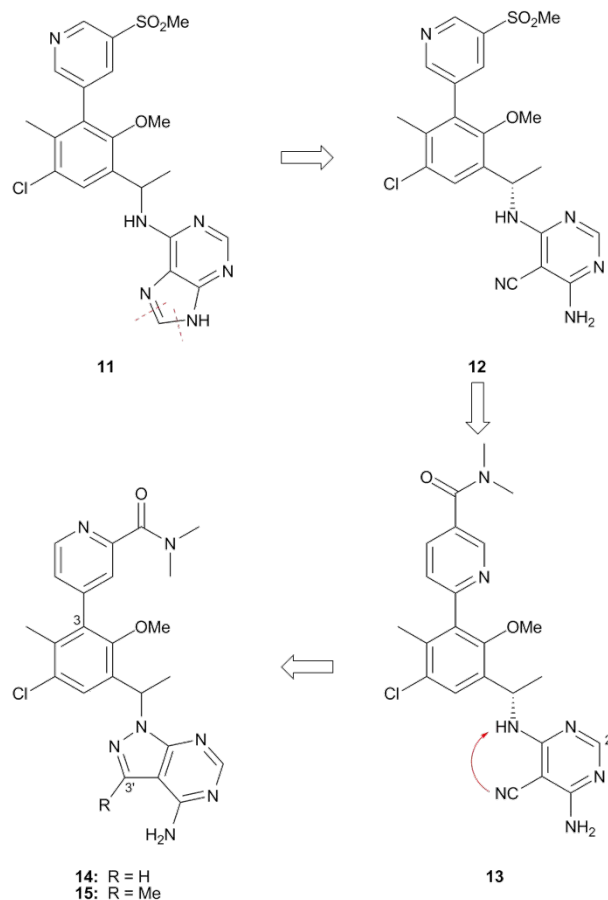


Figure 4. Evolution of purine inhibitor **11** to aminocyanopyrimidine inhibitors **12** and **13** to pyrazolopyrimidine inhibitors **14** and **15**.

carboxamides. The dimethyl amide found in **13** provided the best combination of potency and physical properties with decreased HEK293 and hERG levels. Amide **13** exhibited good oral exposure in rat PK (AUC of $7.7 \mu M \cdot h$ dosed at 4 mg/kg) and was advanced into cyno PK where it surprisingly showed a very short half-life (0.2 h) and very poor oral exposure (AUC of $0.2 \mu M \cdot h$ dosed at 2 mg/kg). A number of other compounds that contained the aminocyanopyrimidine hinge-binder also exhibited poor cyno PK. Metabolic studies revealed that the aminocyanopyrimidine hinge-binder was susceptible to oxidation in cynos by aldehyde oxidase (AO) at the 2'-position. The aminocyanopyrimidine was abandoned and the focus shifted back to hinge-binder optimization.

It was reasoned that blocking the 2'-position of the pyrimidine ring could prevent AO oxidation. Unfortunately, a variety of functional groups that were examined resulted in either loss of potency or compounds that did not have optimal ADME properties (data not shown). Several other monocyclic and bicyclic hinge-binders were examined and the most promising was the pyrazolopyrimidine of **14** which was essentially a cyclized version of the aminocyanopyrimidine (Figure 4). The potency of **14** could be substantially improved with the addition of a methyl group at the 3'-position of the pyrazolopyrimidine (**15**) which resulted in a >100-fold increase in PI3K δ inhibition. The overall profile of **15** appeared encouraging and SAR studies at the 3-position of the central phenyl ring continued with aryl groups. However, a parallel effort to identify saturated rings at the 3-position had initiated

and, in general, provided compounds with better physical properties.

A number of saturated rings were synthesized and selected examples are shown in Figure 5. Excitingly, piperidine **16** was only slightly less potent than pyridyl amide **15** with a similar intrinsic clearance, but **16** had a higher free fraction in human plasma. Azetidines typically had a better profile than piperidines and extensive SAR studies led to azetidine **17**. Compound **17** was very potent in the biochemical and cellular assays and it had a very high free fraction in human plasma that translated into a $PB_{adj} IC_{50}$ in the Pfeiffer assay that was 18-fold more potent than **3**. Compound **17** was studied in rat and cyno PK where it exhibited good oral exposure in rats (AUC of 6.8 $\mu M \cdot h$ dosed at 5 mg/kg) but only moderate oral exposure in cyno (AUC of 4.1 $\mu M \cdot h$ dosed at 1 mg/kg). Initial toxicology studies indicated **17** was tolerated in dogs but, unfortunately, the 28-day investigational new drug (IND)-enabling toxicology study revealed testicular lesions which halted further development.

One challenge observed with saturated heterocycles containing a basic nitrogen was their propensity to inhibit hERG. This could be mitigated with nearby polar groups such as the secondary alcohol found in **17**. Another approach to mitigate hERG inhibition was to remove the basic nitrogen altogether which led to the design of the five-membered lactam ring of **18**. As the result of reduced hERG inhibition and similar potency to **17**, lactam **18** was deemed to be a good lead for further investigation and several analogs (**18-25**) were synthesized (Supporting Information, Schemes S13 – S16). Both diastereoisomers of the lactam ring provided compounds that were potent, although the lactam stereogenic center was usually not assigned. The more potent of the lactam diastereoisomers are presented in Table 2 (**18-21**). The corresponding less potent diastereoisomers (**22-25**) can be found in the Supporting Information.

SAR studies of the lactam series focused around the central phenyl ring. Converting the methoxy of **18** to ethoxy (**19**) resulted in a slight increase in potency. Replacement of the methyl at the 4-position of **19** with fluoro (**20**) resulted in another small boost in potency. The most potent analog was cyano **21** which was about 3-fold more potent in the cellular assays than

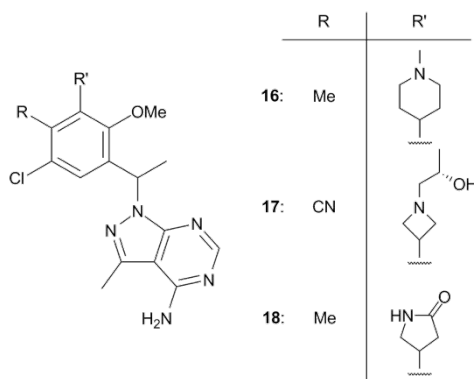


Figure 5. Monocyclic pyrazolopyrimidine inhibitors **16-18** with 3-substituted saturated cyclic rings.

19. The intrinsic clearance of these lactams were all very similar. The cyano analog (**21**) had the highest free fraction (23%), however, it also had the lowest Caco2 permeability (0.3×10^{-6} cm/s). The fluoro analog (**20**), which had the same PB_{adj}

IC_{50} in the Pfeiffer assay as cyano **21**, but with slightly better Caco2 permeability (1×10^{-6} cm/s), offered the best balance of properties. Compound **20** was selected for further profiling which revealed it is potent in the PI3K δ filter binding assay and is very selective over the other PI3K isoforms (Table 3). In addition, **20** exhibits selectivity over a panel of 197 kinases²⁰ and is very potent in the RAMOS cellular and human whole blood basophil assays. Compound **20** did not inhibit hERG or the major isoforms of human cytochrome P450, and it has very good solubility at pH 7.4 (see Supporting Information, Table S13, for additional data).

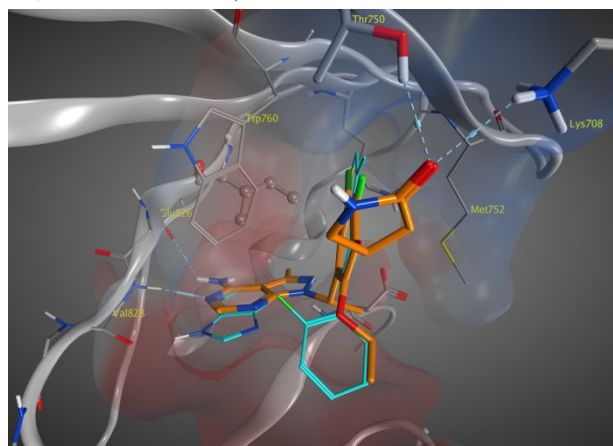


Figure 6. Proposed binding model of **20** (orange) with PI3K δ overlaid with **3** (cyan).

The modeling of **20** with PI3K δ (Figure 6), which was based on the X-ray co-crystal structure (PDB ID 6G6W) of a different inhibitor with PI3K δ ,²¹ revealed a similar induced fit exhibited by other PI3K δ -selective inhibitors.²² The pyrazolopyrimidine in **20** binds the hinge region of PI3K δ forming hydrogen bonds with the NH of Val828 and CO of Glu826. The phenyl ring is positioned in the induced specificity pocket formed by the side chains of Trp760 and Met752, which adopts this alternate conformation to accommodate the phenyl ring. The chloro and fluoro groups on the phenyl ring of **20** effectively mimic the second ring commonly found in the bicyclic core structure of PI3K δ inhibitors (e.g., **3**). The carbonyl of the lactam also forms hydrogen-bonding interactions with both Thr750 and Lys708.

The PK of **20** have been studied in rats, dogs, and monkeys (Supporting Information, Table S20). Following intravenous (IV) administration, **20** displayed low systemic clearance, representing 26%, 2%, and 5% of the hepatic blood flow in rats, dogs, and monkeys, respectively. The steady-state volume of distribution was moderate in rats (1.54 L/kg) and monkeys (0.72 L/kg), but low in dogs (0.32 L/kg). The terminal elimination half-life values were favorable after IV dosing, ranging from 4.0 h (rat) to 7.3 h (monkey) with similar values obtained after oral dosing. Following oral administration **20** was rapidly absorbed with T_{max} (time taken to reach the maximum concentration) values of 0.3 h (rat) to 2.5 h (monkey). Oral exposure was high and the bioavailability of **20** was complete in dogs (100%), and high in monkeys (79%) and rats (74%).

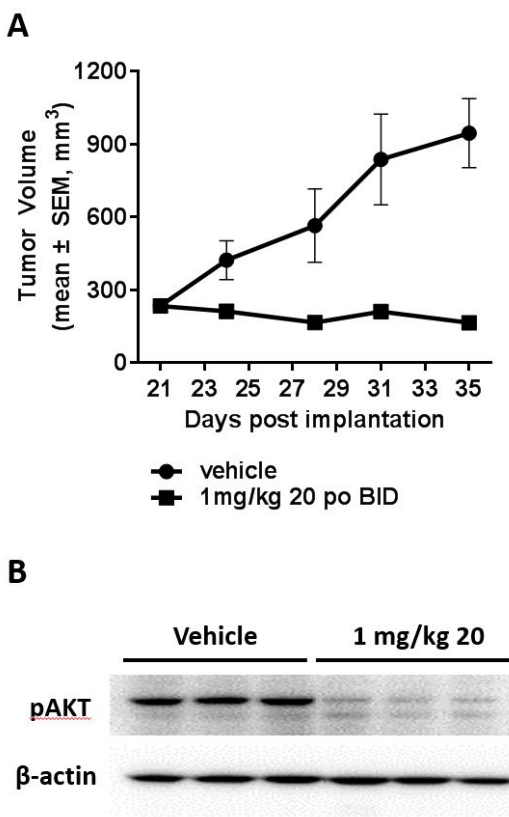


Figure 7. (A) Compound **20** suppresses tumor growth in Pfeiffer mouse xenograft model. Compound **20** was administered orally twice daily for 14 days. The percentage of tumor growth inhibition (TGI) was measured on the final day of study. (B) Analysis of mice from the Pfeiffer xenograft

model revealed inhibition of the phosphorylation of AKT at Ser473.

To determine the effects of **20** in vivo, the Pfeiffer DLBCL subcutaneous mouse xenograft model was used. Pfeiffer cells are highly sensitive to PI3K δ inhibition in vitro with IC₅₀ values for **20** in proliferation and signaling assays less than 5 nM.²⁰ Compound **20** dosed orally twice daily significantly inhibited Pfeiffer xenograft tumor growth at 1 mg/kg (Figure 7A; $p < 0.05$). This correlated with profound inhibition of the phosphorylation of AKT at Ser473, a marker of PI3K δ activity, observed in mice (Figure 7B). Descriptions of additional pharmacologic, pharmacokinetic, and pharmacodynamic analyses in multiple models are described elsewhere.²⁰

Preclinical 28-day IND-enabling toxicology studies in rats and dogs demonstrated no liver toxicities and suggested **20** was suitable for advancement into clinical trials. Thus far, **20** has shown reduced liver-related toxicities in clinical trials,²³ which supports the hypothesis that the hepatotoxicity displayed by **1**, **2**, and **3** could be related to the purine group that is common to all three first-generation compounds.²⁰

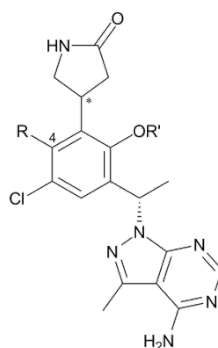
In summary, a potent and selective inhibitor of PI3K δ was discovered. The bicyclic thiazolopyrimidinone core of **3** could be truncated to a single phenyl ring. Replacement of the purine hinge-binder of **3** with pyrazolopyrimidine provided compounds that were slightly more potent with improved cellular permeability. Further optimization revealed the five-membered lactam ring was a good replacement of aryl rings at the 3-position of the core phenyl ring that led to the discovery of **20**. The excellent pharmacokinetics of **20** in various species, its efficacy in inhibiting tumor growth in a Pfeiffer xenograft model, and its lack of preclinical toxicity allowed it to be advanced into clinical development. Parsaclisib (**20**) is currently in Phase 2 clinical trials for the treatment of various cancers.¹⁶⁻¹⁹

Table 1. Selected SAR of 3-17

Cmpd	PI3K δ SPA IC ₅₀ (nM)	SU-DHL-6 Viability IC ₅₀ (nM)	Pfeiffer Proliferation IC ₅₀ (nM)	Pfeiffer PB _{adj} IC ₅₀ (nM)	% f_u in human plasma
3	3.4	18	14	66	17
4^a	430	1800	490	3200	10
5	8.4	140	50	1000	1.4
6	13	73	26	270	5.9
7^a	99	1300	660	ND	0.64
8^a	5.3	60	8.7	ND	ND
9	2.8	100	120	950	2.9
10	3.6	170	130	3100	1.3
11	1.7	14	9.5	40	12
12	0.99	3.1	3.4	17	14
13	1.8	21	17	61	22
14^a	120	840	610	4500	9.2
15	0.93	7.4	8.6	61	8.9
16^a	11	44	11	53	19
17	1.9	2.4	1.5	3.6	42

^aRacemates; ^bdosed at 4 mg/kg or dose adjusted to 4 mg/kg; f_u = fraction unbound; ND = not determined.

Table 2. SAR of Lactam Pyrazolopyrimidines 18-21



Cmpd ^a	*	R	R'	PI3K δ SPA IC ₅₀ (nM)	SU-DHL-6 Viability IC ₅₀ (nM)	Pfeiffer Proliferation IC ₅₀ (nM)	Pfeiffer PB _{adj} IC ₅₀ (nM)	% <i>f</i> _u in human plasma	IntCL (L/h/kg)	Caco2 <i>P</i> _m (x10 ⁻⁶ cm/s)
18		Me	Me	2.4	13	51	480	10	0.7	2.8
19		Me	Et	1.4	2.1	4.8	47	6.5	0.7	1.9
20	<i>R</i>	F	Et	<1.0	1.6	2.5	4.2	5.8	0.7	1.0
21		CN	Et	<1.0	0.47	1.7	4.1	23	0.7	0.3

^aSingle isomers; ^bdosed at 4 mg/kg or dose adjusted to 4 mg/kg; *f*_u = fraction unbound.

Table 3. Summary of InVitro Profile of 20

Assay	Result	N
PI3K δ SPA IC ₅₀ (nM)	<1.0	7
PI3K δ FB IC ₅₀ (nM)	1.1 ± 0.50	11
PI3K α FB IC ₅₀ (nM)	>20,000	4
PI3K β FB IC ₅₀ (nM)	>20,000	4
PI3K γ FB IC ₅₀ (nM)	>10,000	5
SU-DHL-6 IC ₅₀ (nM)	1.6 ± 0.90	22
Pfeiffer IC ₅₀ (nM)	2.5 ± 0.65	8
RAMOS IC ₅₀ (nM)	1.1 ± 0.85	11
WB IC ₅₀ (nM)	2.0 ± 1.2	5
hERG patch IC ₅₀ (nM)	75,000	1
Solubility at pH 7.4 (μg/mL)	210 ± 72	3

■ ASSOCIATED CONTENT

Supporting Information

The Supporting Information is available free of charge on the ACS Publications website at DOI: XXXX. Experimental protocols and characterization data (PDF).

■ AUTHOR INFORMATION

Corresponding Author

*E-mail: eddyue@incyte.com

Current affiliations: P. A. S. and A. P. C., Prelude Therapeutics, Inc., Wilmington, DE, USA; B. M., private consultant, Moraga, CA, USA

ORCID

Eddy W. Yue: 0000-0001-9554-5078

Andrew P. Combs: 0000-0003-1418-5168

Author Contributions:

- Design/conception of study or data acquisition/analysis and/or interpretation: all authors
- Drafting manuscript or providing critical review of content: all authors
- Approval of final draft for publication: all authors
- Accountable for all aspects of work: all authors

Funding Sources: Incyte Corporation, Wilmington, DE, USA

■ ACKNOWLEDGMENTS

This manuscript is dedicated to the memory of our friend and colleague Dr. Yun-Long Li. Yun-Long was a passionate and creative medicinal chemist who initiated the PI3K δ program and led the team that identified INCB040093. The discovery of piasclisib could not have been possible without the pivotal insights from Yun-Long.

We thank Laurine Galya, Mei Li, James Doughty, and Karl Blom for their analytical assistance. We thank Ravi Jalluri for creating the molecular modeling graphics. We thank Jordan Fridman for discussions related to pharmacology. We thank Daniel Levy, Neil Lajkiewicz, and Matthew McCammant for proofreading this manuscript. Medical writing assistance was provided by Simon J. Slater, PhD, CMPP, of Envision Pharma Group (Philadelphia, PA), funded by Incyte Corporation.

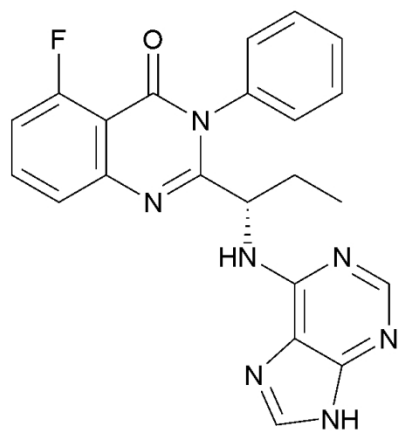
■ ABBREVIATIONS

ADME, absorption, distribution, metabolism, and excretion; AKT, protein kinase B; AUC, area under the plasma drug concentration–time curve; C_{max} , maximum drug concentration; F, fraction of an administered dose of unchanged drug that reaches the systemic circulation; FB, filter binding; hERG, human ether-a-go-go-related gene; IV, intravenous; mTOR, mammalian target of rapamycin; SPA, scintillation proximity assay; $t_{1/2}$, time taken for half the initial dose of medicine administered to be eliminated from the body; $V_{d_{ss}}$, volume of distribution at steady state; WB, whole blood.

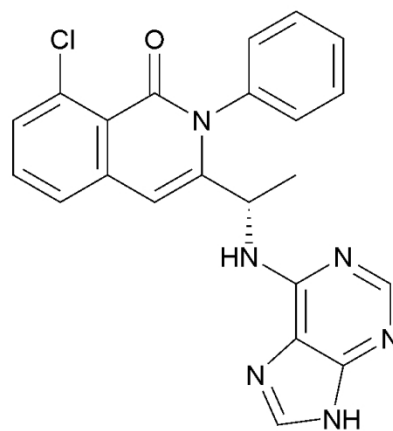
■ REFERENCES

- (1) Vanhaesebroeck, B.; Leever, S. J.; Ahmadi, K.; Timms, J.; Katso, R.; Driscoll, P. C.; Woscholski, R.; Parker, P. J.; Waterfield, M. D. Synthesis and Function of 3-Phosphorylated Inositol Lipids. *Annu. Rev. Biochem.* **2001**, *70*, 535–602.
- (2) Puri, K. D.; Gold, M. R. Selective Inhibitors of Phosphoinositide 3-Kinase Delta: Modulators of B-Cell Function with Potential for Treating Autoimmune Inflammatory Diseases and B-Cell Malignancies. *Front. Immunol.* **2012**, *3*, 1–16.
- (3) Billottet, C.; Grandage, V. L.; Gale, R. E.; Quattropiani, A.; Rommel, C.; Vanhaesebroeck, B.; Khwaja, A. A Selective Inhibitor of the p110 δ isoform of PI 3-Kinase Inhibits AML Cell Proliferation and Survival and Increases the cytotoxic effects of VP16. *Oncogene* **2006**, *25*, 6648–6659.
- (4) Fruman, D. A.; Rommel, C. PI3K δ Inhibitors in Cancer: Rationale and Serendipity Merge in the Clinic. *Cancer Discov.* **2011**, *1*, 562–572.
- (5) Fruman, D. A.; Chiu, H.; Hopkins, B. D.; Bagrodia, S.; Cantley, L. C.; Abraham, R. T. The PI3K Pathway in Human Disease. *Cell* **2017**, *170*, 605–635.
- (6) Michalovich, D.; Nejentsev, S. Activated PI3 Kinase Delta Syndrome: From Genetics to Therapy. *Front. Immunol.* **2018**, *9*, 1–6.
- (7) Stokes, C. A.; Condliffe, A. M. Phosphoinositide 3-Kinase δ (PI3K δ) in Respiratory Disease. *Biochem. Soc. Trans.* **2018**, *46*, 361–369.
- (8) Markham, A. Idelalisib: First Global Approval. *Drugs* **2014**, *74*, 1701–1707.
- (9) Yang, Q.; Modi, P.; Newcomb, T.; Queva, C.; Gandhi, V. Idelalisib: First-in-Class Delta Inhibitor for the Treatment of Chronic Lymphocytic Leukemia, Small Lymphocytic Leukemia, and Follicular Lymphoma. *Clin. Cancer Res.* **2015**, *21*, 1537–1542.
- (10) Blair, H. Duvelisib: First Global Approval. *Drugs* **2018**, *78*, 1847–1853.
- (11) Shin, N.; Li, Y.-L.; Mei, S.; Wang, K. H.; Hall, L.; Katiyar, K.; Wang, Q.; Yang, G.; Rumberger, B.; Leffet, L.; He, X.; Rupar, M.; Bowman, K.; Favata, M.; Li, J.; Liu, M.; Li, Y.; Covington, M.; Koblisch, H.; Soloviev, M.; Shuey, D.; Burn, T.; Diamond, S.; Fridman, J.; Combs, A.; Yao, W.; Yeleswaram, S.; Hollis, G.; Vaddi, K.; Huber, R.; Newton, R.; Scherle, P. INCB040093 is a Novel PI3K δ Inhibitor for the Treatment of B Cell Lymphoid Malignancies. *J. Pharmacol. Exp. Ther.* **2018**, *364*, 120–130.
- (12) Incyte. Study of INCB040093 in Subjects with Previously Treated B-Cell Malignancies. Available from <https://clinicaltrials.gov/ct2/show/NCT01905813>. NLM identifier: NCT01905813. Accessed October 16, 2019.
- (13) Coutré, S. E.; Barrientos, J. C.; Brown, J. R.; de Vos, S.; Furman, R. R.; Keating, M. J.; Li, D.; O'Brien, S. M.; Pagel, J. M.; Poleski, M. H.; Sharman, J. P.; Yao, N.-S.; Zelenetz, A. D. Management of Adverse Events Associated with Idelalisib Treatment: Expert Panel Opinion. *Leuk. Lymphoma* **2015**, *56*, 2779–2786.
- (14) Flinn, I. W.; Patel, M.; Oki, Y.; Horwitz, S.; Foss, F. F.; Allen, K.; Douglas, M.; Stern, H.; Sweeney, J.; Kharidia, J.; Kelly, P.; Kelly, V. M.; Kahl, B. Duvelisib, an Oral Dual PI3K- δ , γ Inhibitor, Shows Clinical Activity in Indolent Non-Hodgkin Lymphoma in a Phase 1 Study. *Am. J. Hematol.* **2018**, *93*, 1311–1317.
- (15) Phillips, T. J.; Forero-Torres, A.; Sher, T.; Diefenbach, C. S.; Johnston, P.; Talpaz, M.; Pulini, J.; Zhou, L.; Scherle, P.; Chen, X.; Barr, P. M. Phase 1 Study of the PI3K δ Inhibitor INCB040093 +/- JAK1 Inhibitor Itacitinib in Relapsed/Refractory B-Cell Lymphoma. *Blood* **2018**, *132*, 293–306.
- (16) Incyte. A Phase 2 Safety and Efficacy Study of INCB050465 in Subjects With Relapsed or Refractory Diffuse Large B-Cell Lymphoma (CITADEL-202). Available from <https://clinicaltrials.gov/ct2/show/NCT02998476>. NLM identifier: NCT02998476. Accessed October 16, 2019.
- (17) Incyte. An Open-Label Study of INCB050465 in Relapsed or Refractory Follicular Lymphoma (CITADEL-203). Available from <https://clinicaltrials.gov/ct2/show/NCT03126019>. NLM identifier: NCT03126019. Accessed October 16, 2019.
- (18) Incyte. A Study of INCB050465 in Subjects With Relapsed or Refractory Marginal Zone Lymphoma (CITADEL-204). Available from <https://clinicaltrials.gov/ct2/show/NCT03144674>. NLM identifier: NCT03144674. Accessed October 16, 2019.
- (19) Incyte. A Study of INCB050465 in Relapsed or Refractory Mantle Cell Lymphoma Previously Treated With or Without a BTK Inhibitor (CITADEL-205). Available from <https://clinicaltrials.gov/ct2/show/NCT03235544>. NLM identifier: NCT03235544. Accessed October 16, 2019.
- (20) Shin, N.; Stubbs, M.; Koblisch, H.; Yue, E. W.; Soloviev, M.; Douty, B.; Wang, K. H.; Wang, Q.; Gao, M.; Feldman, P.; Yang, G.; Hall, L.; Hansbury, M.; O'Connor, S.; Leffet, L.; Collins, R.; Katiyar, K.; He, X.; Waeltz, P.; Collier, P.; Lu, J.; Li, Y.-L.; Li, Y.; Liu, P. C. C.; Burn, T.; Covington, M.; Diamond, S.; Shuey, D.; Roberts, A.; Yeleswaram, S.; Hollis, G.; Metcalf, B.; Yao, W.; Huber, R.; Combs, A.; Newton, R.; Scherle, P. INCB050465 (Parsaclisib) is a Next-Generation PI3K δ Inhibitor with Reduced Hepatotoxicity and Potent Anti-Tumor and Immunomodulatory Activities in Models of B Cell Malignancy. Manuscript submitted.
- (21) Erra, M.; Taltavull, J.; Bernal, F. J.; Caturla, J. F.; Carrascal, M.; Pagès, L.; Mir, M.; Espinosa, S.; Gràcia, J.; Domínguez, M.; Sabaté, M.; Paris, S.; Maldonado, M.; Hernández, B.; Bravo, M.; Calama, E.; Miralpeix, M.; Lehner, M. D.; Calbet, M. Discovery of a Novel Inhaled PI3K δ Inhibitor for the Treatment of Respiratory Diseases. *J. Med. Chem.* **2018**, *61*, 9551–9567.

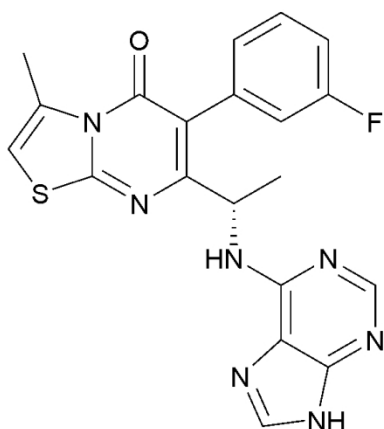
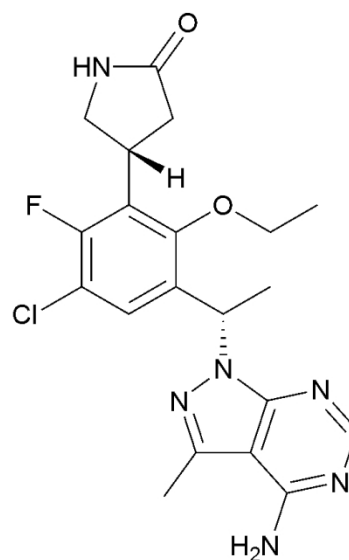
- 1 (22) Berndt, A.; Miller, S.; Williams, O.; Le, D. D.; Houseman, B. T.; Pacold, J. I.; Gorrec, F.; Hon, W.-C.; Ren, P.; Liu, Y.;
2 Rommel, C.; Gaillard, P.; Ruckle, T.; Schwarz, M. K.; Shokat, K. M.; Shaw, J. P.; Williams, R. L. The p110 δ Structure:
3 Mechanisms for Selectivity and Potency of New PI(3)K Inhibitors. *Nat. Chem. Biol.* **2010**, *6*, 117–124.
4 (23) Forero-Torres, A.; Ramchandren, R.; Yacoub, A.; Wertheim, M. S.; Edenfield, W. J.; Caimi, P.; Gutierrez, M.; Akard,
5 L.; Escobar, C.; Call, J.; Persky, D.; Iyer, S.; DeMarini, D. J.; Zhou, L.; Chen, X.; Dawkins, F.; Phillips, T. J. *Blood* **2019**,
6 *133*, 1742-1752.
7
8
9
10
11
12
13
14
15
16
17
18
19
20
21
22
23
24
25
26
27
28
29
30
31
32
33
34
35
36
37
38
39
40
41
42
43
44
45
46
47
48
49
50
51
52
53
54
55
56
57
58
59
60



idelalisib (1)



duvelisib (2)

INCB040093 (3)
dezapelisibINCB050465 (20)
parsacalisib

129x156mm (300 x 300 DPI)

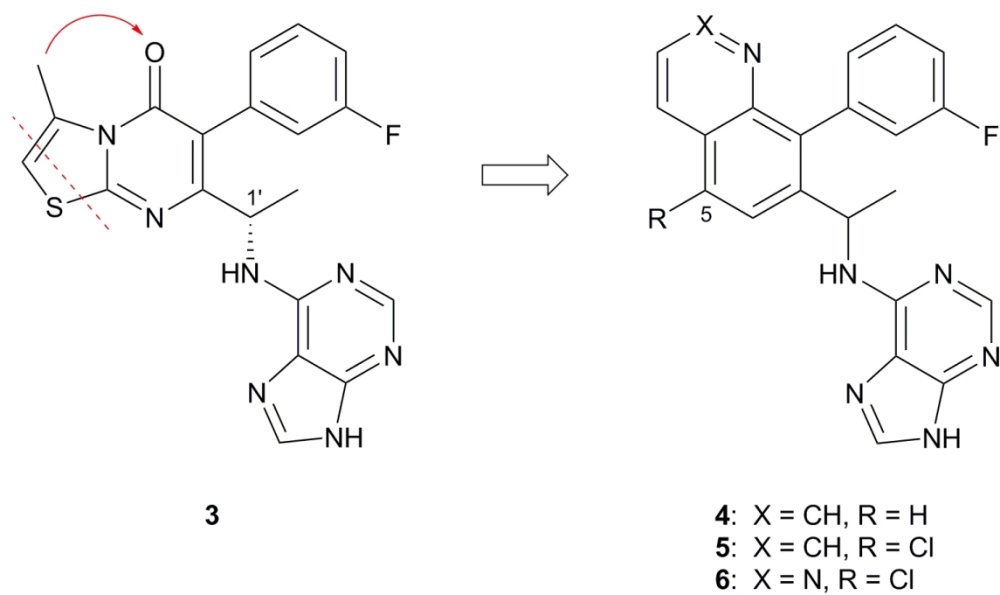


Figure 2

129x76mm (300 x 300 DPI)

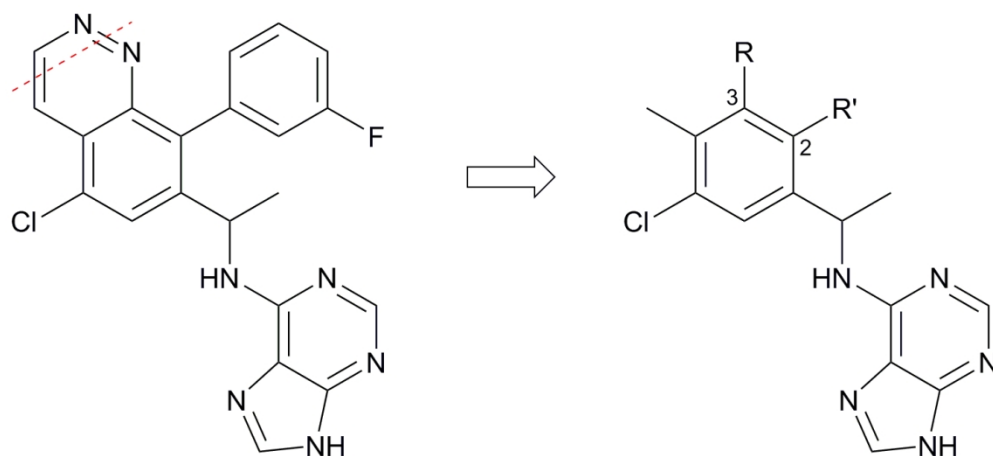
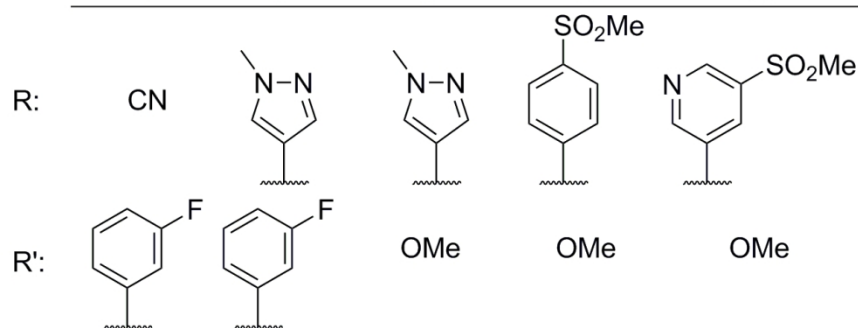
**6****7****8****9****10****11**

Figure 3

125x119mm (300 x 300 DPI)

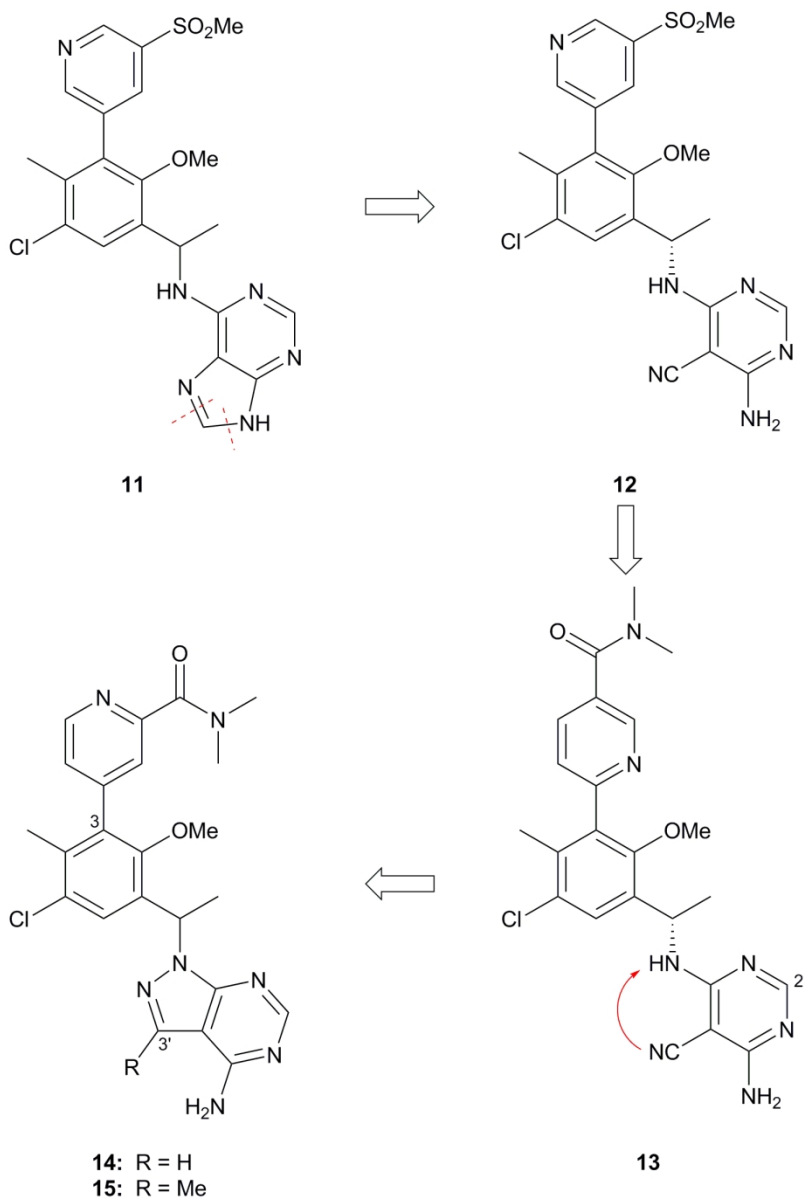


Figure 4

130x192mm (300 x 300 DPI)

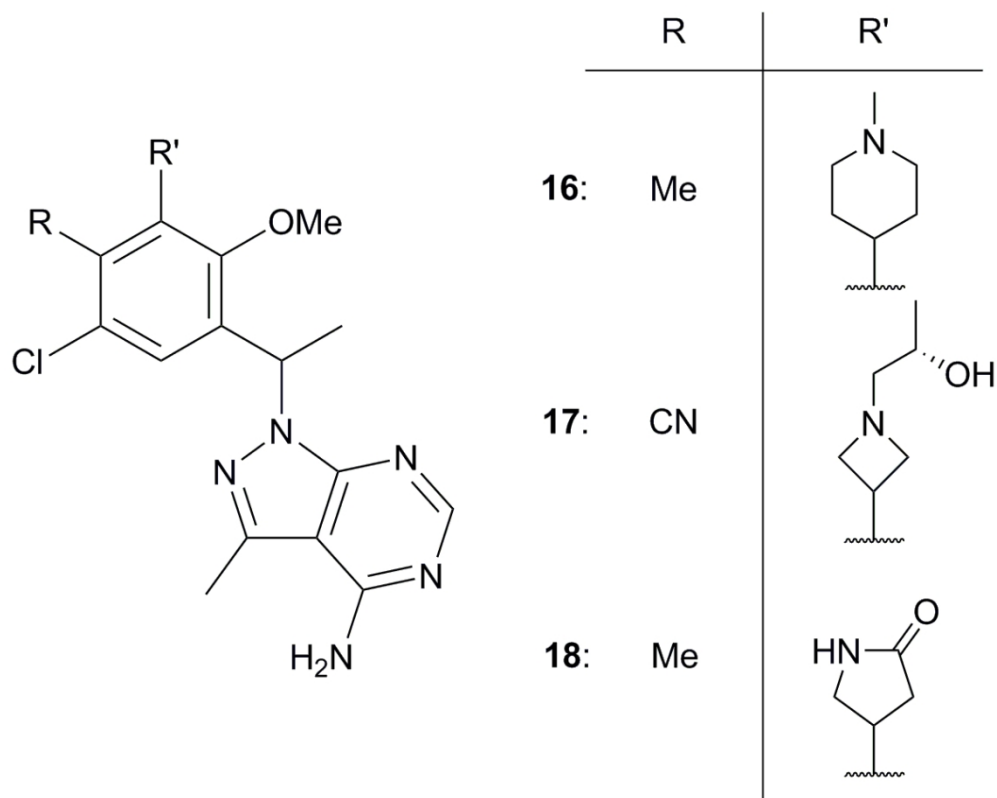


Figure 5

102x81mm (300 x 300 DPI)

1
2
3
4
5
6
7
8
9
10
11
12
13
14
15
16
17
18
19
20
21
22
23
24
25
26
27
28
29
30
31
32
33
34
35
36
37
38
39
40
41
42
43
44
45
46
47
48
49
50
51
52
53
54
55
56
57
58
59
60

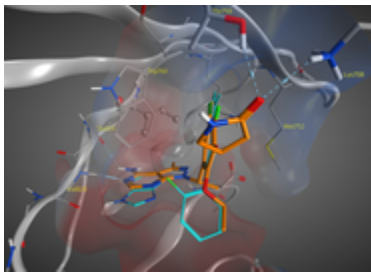


Figure 6

7x5mm (600 x 600 DPI)

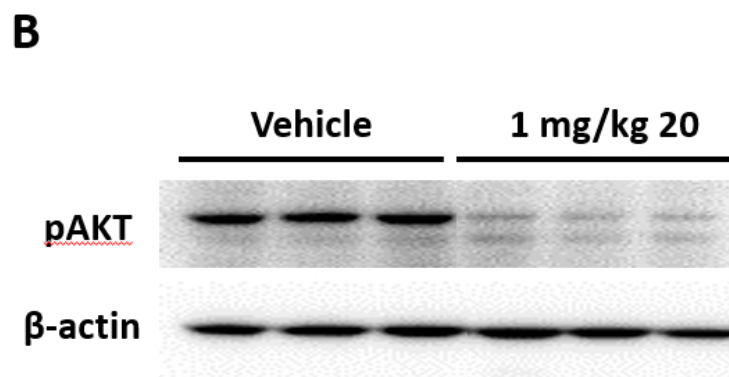
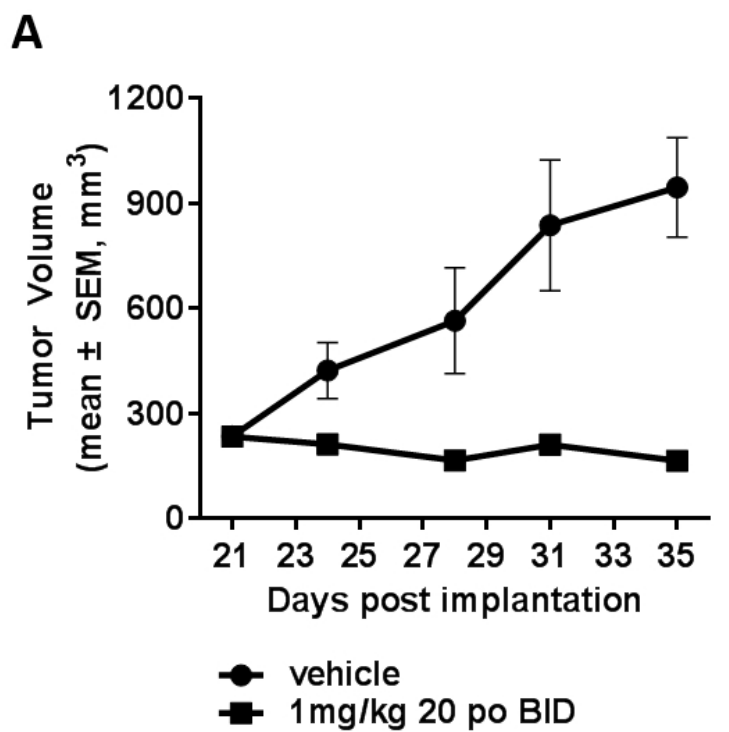


Figure 7

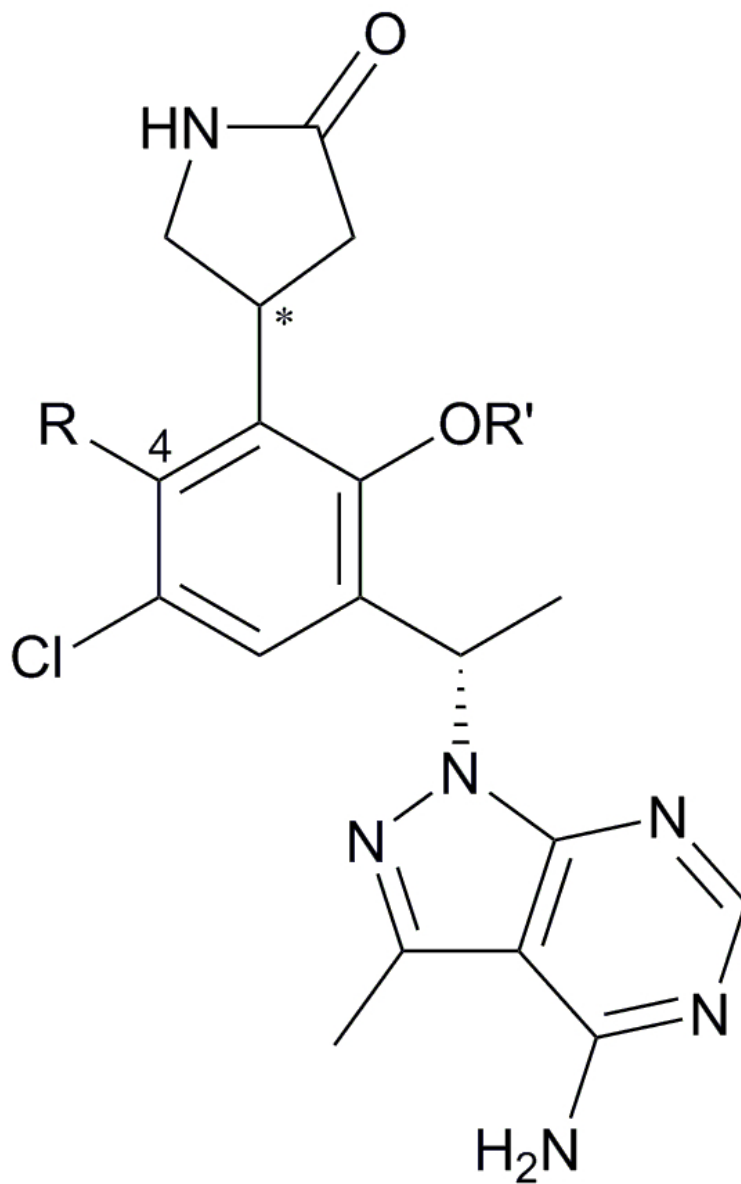
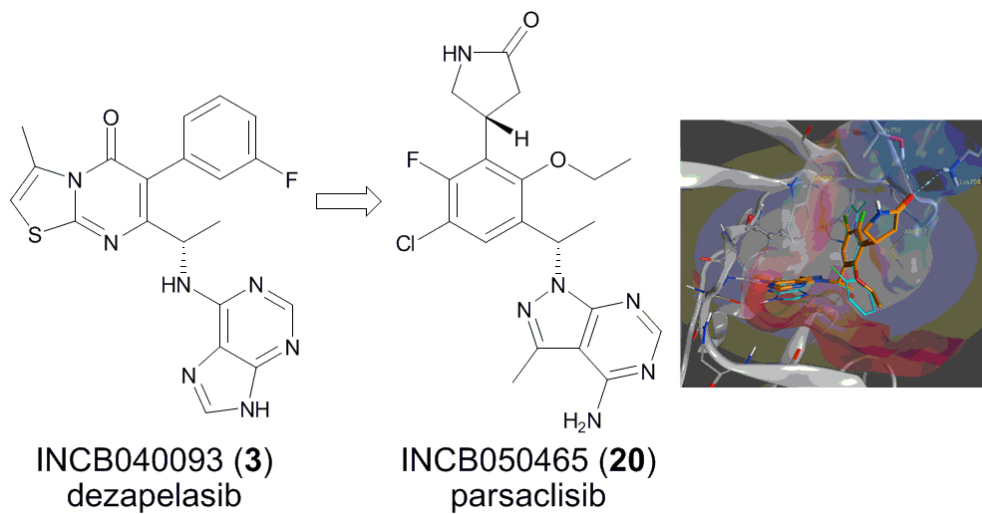


Table 2

46x73mm (300 x 300 DPI)



ToC graphic

84x44mm (300 x 300 DPI)